Pathways to Biorenewable Circularity in Crosslinked Cycloolefin Resins

Zhen Xu,[1] Zi Wang,[1] Maxwell C. Venetos,[2] Sarah Klass,[3, 4, 5,] Pawan Khanal,[2] Christopher W. Chan,[6] Mutian Hua,[1] Jay D. Keasling,[3, 4, 5, 7, 8,] Kristin A. Persson, [1, 2, 9] Brett A. Helms*[1, 3, 9]

1 Materials Sciences Division, Lawrence Berkeley National Laboratory, Berkeley, CA, USA.

2 Department of Materials Sciences and Engineering, University of California Berkeley, Berkeley, CA, USA

3 Joint BioEnergy Institute, Emeryville, CA, USA.

4 Department of Chemical and Biomolecular Engineering, University of California, Berkeley, CA, USA.

5 Biological Systems and Engineering Division, Lawrence Berkeley National Laboratory, Berkeley, CA, USA

6 College of Chemistry, University of California, Berkeley, CA, USA.

7 QB3 Institute, University of California, Berkeley, CA, USA. 5 Biological Systems and Engineering Division, Lawrence Berkeley National Laboratory, Berkeley, CA, USA.

8 The Novo Nordisk Foundation Center for Biosustainability, Technical University Denmark, Kemitorvet, Kongens Lyngby, Denmark.

9 The Molecular Foundry, Lawrence Berkeley National Laboratory, Berkeley, CA, USA.

*Correspondence: bahelms@lbl.gov

Abstract

Crosslinked cycloolefin resins are widely used as thermosets, elastomers, and composites—increasingly so in additive manufacturing—yet crosslinker designs enabling chemical recycling to the original monomers remain obscure. Furthermore, supply chains for raw materials used in cycloolefin resins are volatile due to a combination of geopolitics and growing consumer interest in sustainability. Here, we show how to redesign cycloolefin resins for biorenewable circularity by addressing how bio-derived polar functionality influences ring strain, ring–chain equilibria, and likelihood for catalyst poisoning. These bio-based cycloolefin resins (bioCOR) are thermally and photochemically polymerizable, resulting in high-modulus thermosets with excellent thermal stability. Most notably, we found that the efficacy of thermoset deconstruction to the original crosslinker depended strongly on the ring-closing depolymerization catalyst, where up to 77% yields were achievable with the second generation Hoveyda–Grubbs ruthenium(II) alkylidene catalyst. This showcases the importance of catalyst–polymer interactions in executing circularity with cycloolefin resins, particularly when components of the resin feature bio-derived heteroatoms that would otherwise deactivate catalysts in practice.

Introduction

Cycloolefin resins (CORs) manifest diverse useful properties as thermosets, elastomers, and composites.[1–4] They are also amenable to additive manufacturing using thermal or photochemical processes.[4–8] Yet, crosslinker designs have yet to keep up with demands for more sustainable circular materials. Their reliance on petrochemicals is a growing concern for their

sustainable production, particularly when factories are located in volatile regions around the globe.[9,10] Furthermore, circularity enabling closed-loop chemical recycling of COR-based parts and products at end of life back to their original monomers has also been elusive.[11] Thus, there is urgent need for alternatives that deliver biorenewable circularity.[12–14]

Here, we unite theory with experiment into a workflow that prescribes how to integrate biomolecules into chemically recyclable cycloolefin resins (bioCOR), returning original crosslinkers after catalytic chemical depolymerization (**Figure 1**). This workflow accommodates a broad range of polar functionality in crosslinker designs, owing to the diversity of such compounds in biomolecules and biopolymers. We assess the combined effects of heteroatom placement and ring size on the calculated ring strain energy (RSE) of cycloolefin monomers, revisiting the foundational theoretical methods to include the effects of molecular conformations and solvent effects on circularity. Then, to guide crosslinker design, where monomers are linked together with a bridging biomolecular species, we determine by energy decomposition analysis the interaction energies between polar functionality and open coordination sites at organometallic catalysts, which frames the likelihood of catalyst poisoning, e.g., if a particular bonding motif were used. Using this workflow, we selected for synthesis and validation an amide-based cycloolefin crosslinker whose bridging unit was adipic acid, a bioproduct that is synthesized in a range of microorganisms, e.g., using polyketide synthases.[15] Upon thermal or photochemical polymerization, we obtained high-modulus bioCOR thermosets with excellent thermal stability, showcasing their potential for use in both conventional and additive manufacturing processes. Most notably, when we developed catalysts and processes for bioCOR deconstruction, we found that the yield of the original crosslinker after catalytic deconstruction was strongly influenced by the choice of ring-closing depolymerization catalyst. By using the most efficacious second

generation Hoveyda–Grubbs Ru(II) alkylidene,[16,17] we retrieved the original bioCOR crosslinker in 77% isolated yield.

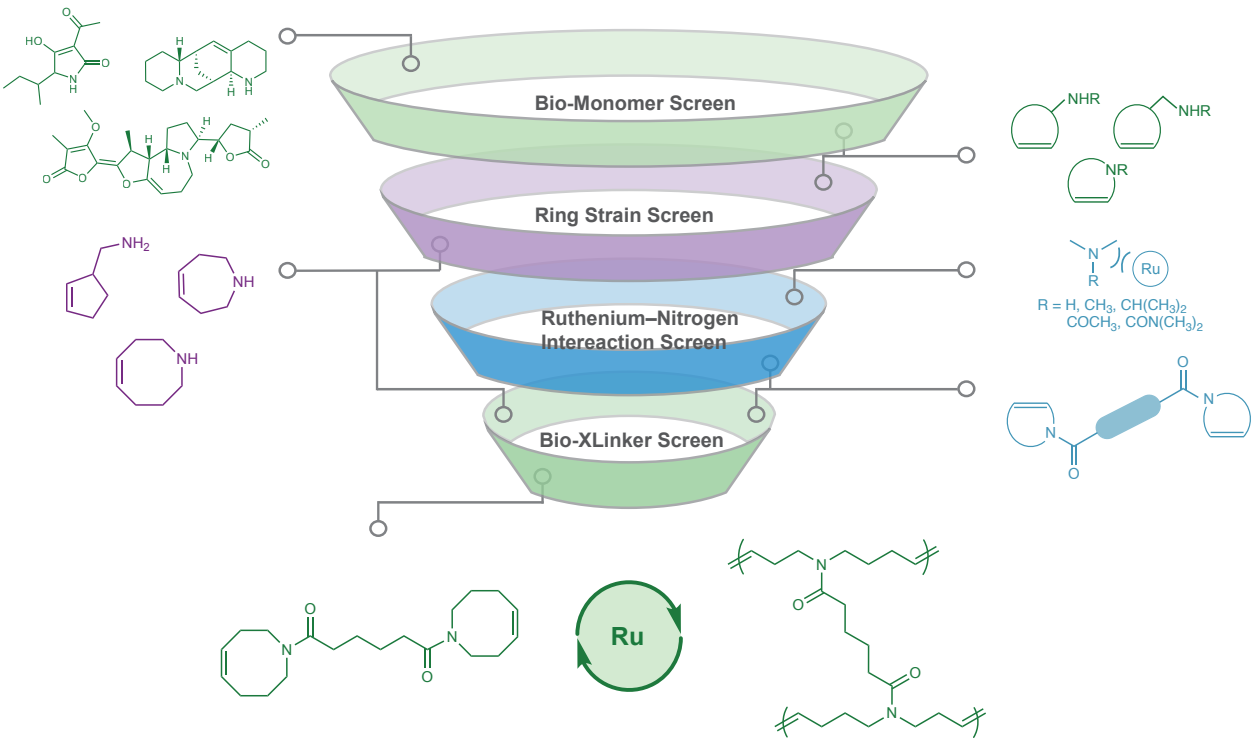

Figure 1. Computational workflow for down-selecting monomers, crosslinkers, catalysts, and polymerization/depolymerization processes enabling biorenewable circularity in crosslinked cycloolefin resins.

Our work complements a broad pallet of degradable CORs thermosets featuring chemically cleavable functionalities, which when cleaved produce structurally non-uniform recyclates.[3,8,18–22] While these recyclates are not the original crosslinkers, they can in some cases be mixed up to 16–25% with virgin monomer materials in subsequent materials generations to deliver similar properties as the first generation; it remains unclear for how many generations this might be allowable. On the other hand, a growing number of cycloolefin monomers, but not crosslinkers, enable circularity in cycloolefin polymers with linear polymer architectures, e.g., by balancing

ring-strain energy in fused ring monomers.[11,23–31] Nevertheless, it remains a significant challenge to bring circularity to highly crosslinked COR thermosets. Also lacking has been insights into creating sustainable supply chains for the raw materials for formulating biorenewable circular CORs. For example, biobased cycloolefin monomers replacing their exact petrochemical counterparts are known,[32] which are examples of polymerizable bio-based CORs with altered designs. However, these alternative designs have poor depolymerizability due to their high ring strain energy,[32] indicating circularity in bioCORs has been out of reach until now.

Results

The ability to incorporate polar functionality via heteroatoms into cycloolefin monomers and crosslinkers is a key to unlocking biorenewable circularity in CORs, given the prevalence of such motifs in biomolecules and biopolymers. Searching through literature, we noticed a variety of natural products featuring amino-cycloolefins (**Figure 2a**). In addition, Nature can produce cycloolefins with various ring sizes, including five-membered (Tenuazonic acid,[33] Jamaicamide A,[34] and Supinidine[35]), seven-membered (Benzastatin K,[36] Securinine,[37] and Dehydroprotostemonine[37,38]) and eight-membered rings (Aloperine,[39] Coelimycin P1,[40] and Hobarine[40,41]). As well, both exocyclic and endocyclic amines can be biosynthesized by natural microorganisms. It has also been shown that amino-cycloolefins can be biosynthesized by utilizing unnatural hybrid polyketide synthases (PKSs).[42] Given the modular nature of PKSs, it becomes possible to generate various amino- and amido-cycloolefin compounds by the programmable installation of PKS modules that can target a range of ring sizes and different placement of nitrogen on the ring. While this consideration is useful in establishing bio-feasibility of amino-cycloolefins, there is no guidance on which bioproducts to prioritize for biosynthesis, if circularity was the key

consideration. Specifically, amino-cycloolefins have not been evaluated for their propensity toward forward or reverse polymerization using various metathesis catalysts. Yet, this knowledge is crucial for the advancement of bioCORs.

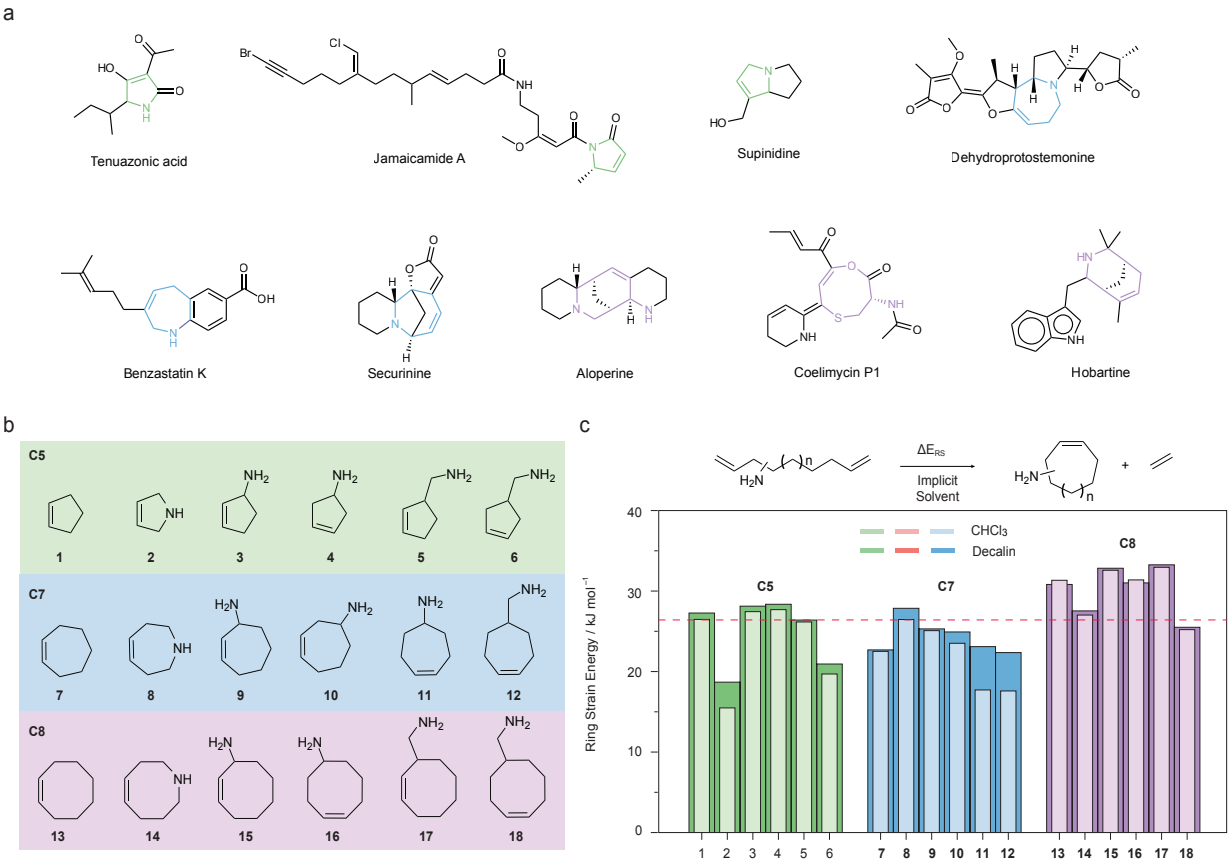

Figure 2. Biosynthetic feasibility of amino-cycloolefins and the library of amino-cycloolefin monomers for RSE calculations. a, Natural products containing desired 5,7, and 8-member amino-cycloolefins. **b**, Library of amino-cycloolefin monomer targets. **c**, Ring strain energies calculated for the library of amino-cycloolefin monomers, compared to hydrocarbon cycloolefin rings. Ring strain energies were calculated in implicit solvent environment, approximating polymerization (decalin) and depolymerization ($CHCl_3$) conditions.

Given the multitude of pathways for the bioproduction of amino-cycloolefins, we were interested in quantifying how nitrogen atom placement and ring size influence circularity via their ring strain energies (RSE) (**Figure 2b**). We considered a series of five- (**1**–**6**), seven- (**7**–**12**), and eight-membered (**13**–**18**) ring monomers. Six-membered rings were excluded due to their negligible ring strain and low polymerizability.[27] We calculated RSE using the enthalpy change of the ring-closing metathesis reaction to produce the target cycloolefin (**Figure 2**). To modernize the approach, we took into account contributions from different conformers using the Conformer–Rotamer Ensemble Sampling Tool (CREST) algorithm.[43] We undertook this for both cycloolefins and their acyclic diene counterparts, while also considering the effects of implicit solvent fields with the SMD solvent model to simulate both forward polymerization in apolar media (modeled as decalin) and reverse depolymerization in polar media (modeled as $CHCl_3$).[44]

Our calculated RSE values of cyclooctene in decalin and $CHCl_3$ are 30.8 and 31.3 kJ mol^{-1}, respectively; the reported value obviating implicit solvent considerations is 31.0 kJ mol^{-1}. Similarly, we calculated RSE for cyclopentene in decalin (27.3 kJ mol^{-1}) and $CHCl_3$ (26.5 kJ mol^{-1}) for comparison to the reported value of 28.5 kJ mol^{-1}, which did not consider solvent.[47] These comparisons to well-studied cycloolefins give confidence in our methods and provide new context to understand the impacts of conformation and solvent effects on bioCOR circularity as they are influenced more broadly by ring size and site of amino-functionalization.

Using these benchmarked methods, we found that amination of cycloolefin ring monomers had a demonstrable influence on RSE. For example, by comparison to ideally circular cyclopentene (**1**) ($RSE_{decalin}$ = 27.3 kJ mol^{-1}), 2,5-dihydro-1*H*-pyrrole (**2**) has a low $RSE_{decalin}$ of 18.7 kJ mol^{-1}, indicating circularity with **2** should be out of reach due to poor polymerizability. $RSE_{decalin}$ values for seven-membered ring monomer 2,3,6,7-tetrahydro-1*H*-azepine (**8**) and eight-

membered ring monomer 1,2,3,4,7,8-hexahydroazocine (**14**) were, on the other hand, 27.9 kJ mol^{-1} and 27.5 kJ mol^{-1}, respectively. Because these values were only marginally higher than that of cyclopentene **1**, amino-functionalization at those sites in larger ring sizes would not be expected to affect polymerizability. With respect to depolymerization, **2** exhibited a low RSE of 15.5 kJ mol^{-1} in $CHCl_3$, indicating that the ring–chain equilibrium would favor depolymerization. Compounds **8** and **14** showed RSE values of 26.5 kJ mol^{-1} and 27.0 kJ mol^{-1}in $CHCl_3$, respectively. Their RSE values were comparable to that of **1** in CHCl3 (26.5kJ mol^{-1}), showcasing their potential ability to depolymerize. In summary, both **8** and **14** are potential candidates for circularity based on our RSE calculations.

We further compared amino-cycloolefins **8** and **14** with their all-hydrocarbon counterparts. We observed an enhancement of RSE in $CHCl_3$ of **8** (26.5 kJ mol^{-1}), compared to cycloheptene (**7**) (22.5 kJ mol^{-1}). Conversely, in eight-membered ring monomers, RSE values in $CHCl_3$ decreased from 31.3 kJ mol^{-1} for cyclooctene (**13**) to 27.0 kJ mol^{-1} for **14**. These results indicated that amino-cycloolefins provide new paths to tune RSE values relevant to circularity, beyond conventional structural motifs such as fused-ring cycloolefins.

These results inspired us to further explore amino-cycloolefin motifs and understand how nitrogen atom placement affect RSE values (**Supplementary Table 1**). By comparing cycloolefin monomers featuring an exocyclic amine to cyclopentene in both decalin and $CHCl_3$, we observed that among these six compounds—**3**, **4**, **9**, **10**, **11**, **15** and **16**—none was predicted to be viable for circularity. In addition, by comparing calculated RSE values in $CHCl_3$, we found that ring size governed the sensitivity of RSE on the relative positions of the olefin and amine. In five-membered ring monomers, RSE did not depend strongly on those relative positions: cyclopent-2-en-1-amine **3** vs. cyclopent-3-en-1-amine **4** (27.4 kJ mol^{-1} vs. 27.7 kJ mol^{-1}). In seven-membered ring

monomers, the dependence was pronounced, where RSE values in $CHCl_3$ decreased from 25.1 kJ mol^{-1} for cyclohept-2-en-1-amine **9** to 23.5 kJ mol^{-1} for cyclohept-3-en-1-amine **10** and then to 17.7 kJ mol^{-1} for cyclohepent-4-en-1-amine **11**. In eight-membered rings, the analogous decrease in RSE with increasing olefin–amine separation was only slight: e.g., 32.6 kJ mol^{-1} for cyclooct-2-en-1-amine **15** to 31.4 kJ mol^{-1} for cyclooct-4-en-1-amine **16**.

When cycloolefins were instead functionalized with methanamine, we observed that RSE depended strongly on the relative positions of the olefin and methanamine in both five- and eight-membered cycloolefins. In five membered ring monomers, cyclopent-2-en-1-ylmethanamine (**5**) exhibited a RSE in decalin of 26.4 kJ mol^{-1}, by comparison to the RSE of cyclopent-3-en-1-ylmethanamine (**6**) (20.9 kJ mol^{-1}). In eight-membered ring monomers, when olefin was placed at 4′ position in cyclooct-4-en-1-ylmethanamine (**18**), the RSE in decalin was calculated as 25.2 kJ mol^{-1}, indicating poor polymerizability. Meanwhile, cyclooct-2-en-1-ylmethanamine (**17**) was predicted to have good polymerizability with a RSE of 33.3 kJ mol^{-1} in decalin, while its high RSE value of 33.0 kJ mol^{-1} in $CHCl_3$ made backward depolymerization unlikely to occur. In summary, when cycloolefins were functionalized with exocyclic methanamine (**5**, **6**, **17**, **12** and **18**), only **5** showed the desirable RSE value for circularity. Among all compounds screened, **5**, **8** and **14** were predicted to fulfill RSE requirements for circularity. To test this hypothesis, we advanced monomer **14** for further investigation.

Having selected monomer **14** for further investigation, we sought to elucidate the interaction between the ring monomer and a prototypical ruthenium(II) alkylidene catalyst featuring an *N*-heterocyclic carbene ligand, which are common in ring-opening polymerization catalysts as well as ring-closing metathesis catalysts and ring-closing metathesis depolymerization catalysts. We sought to identify the optimal bridging biomolecular species for the crosslinker that

would facilitate both polymerization and depolymerization, while avoiding catalyst poisoning.[48–50] We systematically screened several common amine-containing structural motifs, employing energy decomposition analysis to analyze the interaction between the nitrogen atom and catalyst ruthenium(II) alkylidene center (**Figure 3a**).[51] We delineated the contributions of three types of interactions, including frozen contributions, polarization interactions, and charge transfer interactions in the energy decomposition analysis. As a control, we compared the interactions for these polar structural motifs with those of an ethene unit, which are favorable enough with the ruthenium(II) alkylidene center to trigger metathesis reversibly.

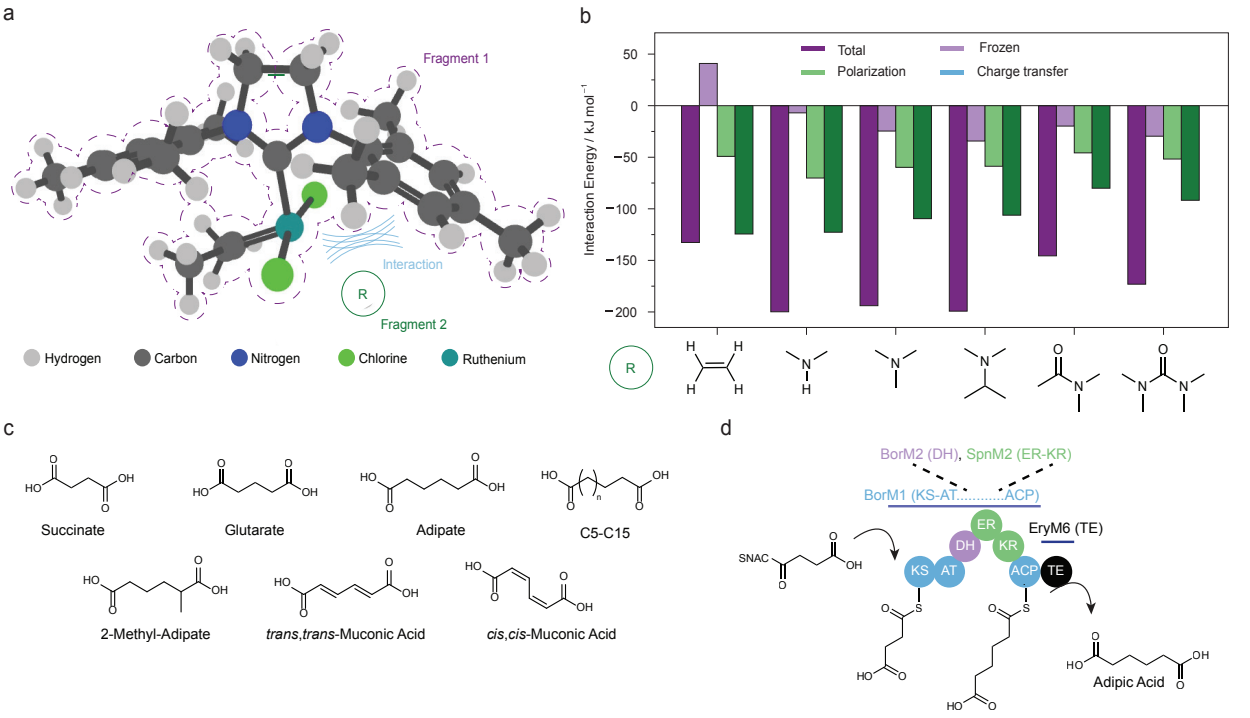

Figure 3. Catalyst–Monomer interactions assessed by energy decomposition analysis informs the design of bridging biomolecular species in bioCOR crosslinkers. a, Interactions between fragments of ruthenium(II) alkylidene catalyst and various small-molecules. **b**, Energy decomposition analysis of interactions between the catalyst and various nitrogen-containing

structural motifs. **c**, Chemical structures of biobased diacids. **d**, Module design for hybrid polyketide synthases (PKSs) that produce adipic acid from succinate precursors.

We first considered the frozen contributions, which refer to steric, Pauli exclusion, and point-charge interactions (**Figure 3b**). Ethene had strong repulsive frozen interactions with the ruthenium(II) center (40.9 kJ mol^{-1}), while dimethyl amine showed a negative interaction energy of –6.97 kJ mol^{-1}. By increasing the steric bulk at nitrogen in trimethylamine and dimethylisopropylamine, frozen interactions became more favored: –24.6 kJ mol^{-1} for trimethylamine; –34.3 kJ mol^{-1} for dimethylisopropylamine. Introducing an amide group led to less negative frozen interaction energies, compared to that of dimethylisopropylamine: –19.8 kJ mol^{-1} for *N*,*N*-dimethylacetamide; –29.6 kJ mol^{-1} for 1,1,3,3-tetramethylurea. We also considered the polarization energy as it depended on the polarization of electronic density during the interaction between the two species. By increasing the steric bulk from dimethylamine, trimethylamine, dimethylisopropylamine to dimethylacetamide, the polarization energies became less negative: i.e., –70.2, –59.9, –58.8, and –45.8 kJ mol^{-1}, respectively. The polarization interaction between ethene and ruthenium(II) was –49.2 kJ mol^{-1}. Notably, frozen and polarization interactions exhibited the opposite trend by increasing the steric bulk at the nitrogen atom.

In addition, we calculated the charge transfer interaction energies, which can be considered as the main indicator for bond formation. Among all selected nitrogen-containing structural motifs, the amide showed the least negative charge transfer energy of –80.0 kJ mol^{-1}. Conversely, the less sterically hindered structural motifs such as dimethylamine exhibited a charge transfer energy of –122.7 kJ mol^{-1}, while trimethylamine and dimethylisopropylamine showed charge transfer energies of –109.6 and –106.2 kJ mol^{-1}. In summary, dimethylacetamide gave the least total

interaction energy of –145.6 kJ mol^{-1}, comparable to that of ethene (132.6 kJ mol^{-1}). Other structural motifs exhibited much higher interaction energies of –199.8 kJ mol^{-1} (dimethylamine), –193.9 kJ mol^{-1} (trimethylamine), –199.2 kJ mol^{-1} (dimethylisopropylamine) and –173.1 kJ mol^{-1} (1,1,3,3-tetramethylurea). Informed by these computational screens, we surmised that an amide moiety was the least likely to poison the catalyst.

To bridge two amino-cycloolefin monomers as an amido-cycloolefin crosslinker, a bio-based diacid is required. Bioproduction of diacids has been well established, ranging from succinic acid (C4),[52] glutaric acid (C5)[53], adipic acid (C6)[54–56] to C15 diacid[57–59] (**Figure 3c**). In addition, modifications of diacids by either side-chain incorporation or reduction to form olefins have been reported, resulting in a diverse selection of biobased diacids for crosslinker design.[56] To avoid cross reactions with the metathesis catalyst, we opted to prioritize aliphatic diacids.

To that end, we have previously reported an engineered pathway employing hybrid polyketide synthases (PKSs) to produce adipic acid (**Figure 3d**).[54] In this hybrid PKS system, a succinyl-SNAC analog, mimicking the loading module acyl carrier protein (ACP) of various PKSs, is loaded and extended. We carried out the extension by a hybrid PKS where specific domains within the extension module are recombined from different PKS modules, including Borrelidin module 1 (BorM1), Borrelidin module 2 (BorM2), Spinosad module 2 (SpnM2), and the Erythromycin thioesterase (EryTE). This hybrid PKS facilitates a fully reduced C2 extension, resulting in the production of adipic acid from the succinyl-SNAC substrate.[54] Thus, adipic acid emerged as a validated target for our initial exploration as the bridging biomolecular species. Using this information about monomer design and bridging biomolecular species, we then designed crosslinker **bioXL**. We synthesized crosslinker **bioXL** in 68% isolated yield from 1,2,3,4,7,8-hexahydroazocine and adipic acid using tetramethyl orthosilicate (TMOS) as the coupling agent.[60]

To verify the thermal polymerizability of **bioXL**, we used the Grubbs 2nd catalyst (G2) due to its high reactivity towards ring-opening metathesis polymerization and its excellent functional group tolerance.[16,17] With 0.5 mol% G2 at 60 °C for 12 h (neat), we synthesized crosslinked thermoset **bioCOR 1,** whose gel fraction was 90%. This confirmed our first hypothesis that the calculated value for RSE should promote ROMP for **bioXL**, because of its similarity to ideally circular cyclopentene. In stride, this confirmed our second hypothesis that in the absence of strong interactions with the catalyst, amide linkages in the crosslinker design should not adversely affect polymerization.

To verify the photochemical polymerizability of crosslinker **bioXL**, we used the ruthenium photocatalyst (1,3-dimesitylimidazolidin-2-ylidene)dichloro(2-((2-ethoxy-2-oxoethylidene)amino)benzylidene)ruthenium(II) (HeatMet) paired with a photosensitizer, isopropylthioxanthone (ITX) (**Figure 4a**). This pairing is known to enable fast photopolymerization of CORs and has been used in additive manufacturing settings such as stereolithography.[5–7] Here, the gel fraction varied with catalyst loading. To deliver a gel fraction of 93%, we prepared **bioCOR 2** using 1 mol% HeatMet and 0.75 mol% ITX; lowering the catalyst loading to 0.5 mol% resulted in a gel fraction of 80%.

For both thermally and photochemically polymerized **bioCOR** resins, we measured the glass transition temperatures (T_g) using differential scanning calorimetry (DSC) (Figure 4b): T_g for thermally polymerized **bioCOR 1** was at 42 °C; T_g for photochemically polymerized **bioCOR 2** was 47 °C. We also determined the decomposition temperature (T_d) of **bioCOR 1 & 2** by using thermogravimetric analysis (TGA): while thermally polymerized **bioCOR 1** exhibited a T_d of 300 °C, photopolymerized **bioCOR 2** showed a higher T_d at 360 °C (**Figure 4c**).

We further conducted rheological characterization of **bioCOR 1** to understand its dynamic thermomechanical behaviors. We found in the frequency and amplitude sweep measurements quantifying the storage modulus (G') and loss modulus (G'') that there was no crossover point in G'/G'' over the measured ranges (**Figure 4d** & **4e**). Both G' and G'' dropped precipitously beyond 0.01% strain, while storage modulus increased steadily with frequency. The storage modulus was 5.6 MPa at 25 °C and decreased with increases in temperature. We further conducted the temperature sweep and calculated tanδ values by the ratio of G' and G''. The maximum of tanδ is often concurrent with T_g. We obtained tanδ traces with a maximum around 40 °C, i.e., consistent with DSC measurements.

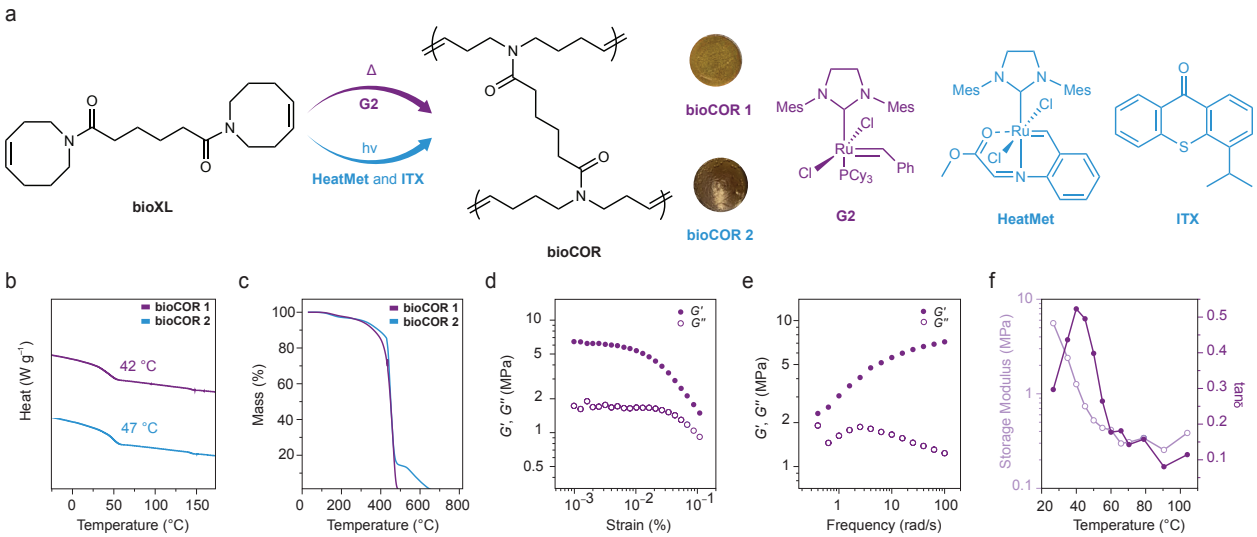

Figure 4 Thermal and photo-polymerization of bioXL and thermomechanical characterizations. a, Chemical structures of amido-cycloolefin crosslinker **bioXL** and the catalyst systems used to either thermally or photochemically cure **bioCOR 1** & **2**, respectively. Photos show bioBOR thermosets after curing. **b**, DSC traces of thermally and photochemically crosslinked **bioCOR 1** & **2**, respectively. **c**, TGA thermograms of thermally and photochemically crosslinked **bioCOR 1** & **2**, respectively. **d**–**f**, Rheological characterization of thermally and

photochemically crosslinked **bioCOR 1** & **2**, respectively: (d) amplitude sweep, (e) frequency sweep, and (f) temperature sweep.

To verify our theoretical predictions that **bioCOR** resins return original amido-cycloolefin crosslinker **bioXL** after ring-closing metathesis depolymerization, we considered the implications of ring–chain equilibria as well as catalyst–polymer interactions on the round-trip efficiency,[23] in terms of time, energy inputs, and isolated yield of the crosslinker. For example, from Jacobsen–Stockmayer theory,[61] ring monomers are accessible by carrying out ring-closing metathesis depolymerization at sufficiently high dilution, i.e., the inverse of polymerization in neat or concentrated solutions of crosslinker. Similarly, with regard to catalyst choice for the thermoset deconstruction process, it is important that ligands at the metal center promote ring-closing over ring-opening. This motivated our selection of catalysts to Hoveyda–Grubbs 2nd generation catalyst (**HG2**), because it has been shown to have outstanding catalytic activity in ring-closing metathesis of small molecules, outperforming **G2**.[62] Notably, **HG2** contains a styrenyl ether bidendate ligand and can undergo ligand release and recapture to inhibit catalyst decomposition (i.e., via a boomerang mechanism).[63] We selected **bioCOR 1** as the test substrate for understanding deconstruction outcomes along these axes of interest.

We carried out thermal ring-closing metathesis depolymerization of **bioCOR 1** in $CDCl_3$ ([**bioXL**] = 12.5 mM) at 60 °C in the presence of 2 mol% **G2** or **HG2** for 24 h (**Figure 5a–c**). Due to the heterogeneous nature of the reaction for thermoset deconstruction, we found that higher temperature and longer reaction times were needed by comparison to cycloolefin thermoplastics, whose monomers have similar RSE values to our crosslinking functionality.[11] The extent of reaction for **bioCOR 1** was 82% with **HG2** (**Supplementary Figure 1**). Remarkably, the crude

^{1}H NMR spectrum was nearly identical to the spectrum for pristine **bioXL** (**Figure 5b**). In contrast, **bioCOR** deconstruction using **G2** led to an extent of reaction of only 20%. Thus, **HG2** is a substantially more effective ring-closing metathesis catalyst with high turnover number due to its boomerang mechanism, which can be translated to its ability to catalyze ring-closing depolymerization with less deactivation over prolonged depolymerization times at elevated temperature. Similarly, due to the absence of strong interactions with the catalyst, amide linkages in the crosslinker design did not adversely affect depolymerization.

We purified the crude depolymerization mixture from the **HG2** deconstruction reaction, which resulted in a 77% isolated yield of crosslinker **bioXL**, whose identity and purity was also quantified by analytical high-performance liquid chromatography–mass spectrometry (HPLC-MS) (**Figure SX**). Similar to observations by Moore and co-workers,[64] a minor impurity appears in the recyclate (less than 9%) whose molecular mass 16 units higher than that of **bioXL** (**Supplementary Figure 2-4**). This has been attributed to the oxidation of cycloolefins, which occurs slowly when samples are stored in air. Nonetheless, we reused and thermally repolymerized recycled amido-cycloolefin crosslinker **bioXL** into second-generation thermosetting materials: **recycled bioCOR 1** exhibited a T_g of 39 °C, favorably comparable to that of first-generation **pristine bioCOR 1** (**Figure 5d**). These results demonstrated that our integrated computational and experimental workflow and **bioXL** and **bioCOR** designs deliver on the promise of closed-loop recycling circularity in crosslinked cycloolefin resin thermosets.

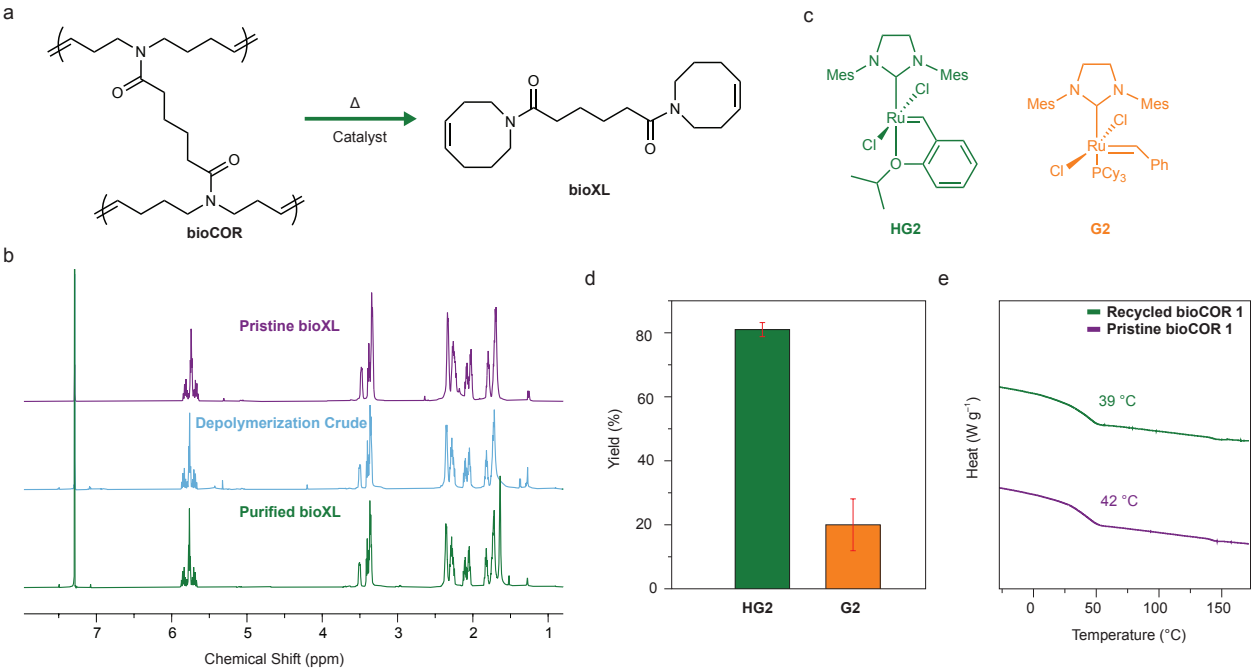

Figure 5. Depolymerization of bioCOR1. **a**, Chemical structures of the closed-loop chemical depolymerization from **bioCOR 1** to **bioXL**, i.e., the original crosslinker. **b**, Overlay of ^{1}H NMR spectra of pristine **bioXL**, crude depolymerization mixture using **HG2** as the catalyst and purified depolymerization product. **c**, Chemical structures of catalysts used in the depolymerization studies and the bar graph of NMR yields using **G2** and **HG2**. **d**, DSC curves of repolymerized materials **recycled bioCOR 1** compared to **pristine bioCOR 1**.

Discussion

Our findings demonstrate that our integrated computational workflow is remarkably capable of predicting novel bio-inspired and bio-based designs for circular cycloolefin resins, especially for crosslinked cycloolefins resins, which have been largely out of reach. We find that in addition to gas-phase ring strain energy calculations, which have been the workhorse for the field, it's important to take into account the range of molecular conformation available to each

species as well as the solvent (implicitly) in which polymerization and depolymerization will likely be taking place, as RSEs are found to be variable in those cases. Implicit solvent models appear to be sufficient at this time, however, in the future, explicit solvent models may become necessary to account for explicit, intermolecular interactions on monomer conformations, energies, and landscapes. Furthermore, to inform the likelihood for crosslinking and depolymerization, crosslinker–catalyst interactions must be taken into account to avoid catalyst poisoning. We recommend EDA for this purpose and presently, it appears sufficient to consider in isolation specific bonds represented in the monomers and crosslinkers that may interact with the metal center. By benchmarking the theoretical predictions with experiment, we find validity in our design concept and implementation in practice. Yet, it's important to recognize that catalyst–polymer interactions may be a further consideration to include in the maturation of workflow to maximize the yield of monomer and crosslinker recovery. Nonetheless, we now have validated biomolecular amino-cycloolefin targets for future biosynthesis activities via PKSs or other pathways to bring about their production at commercial scale; the technology for bio-based diacid production in microorganisms is already established and can be deployed when needed. In this way, sustainable engineering materials for future manufacturing based on biorenewable circular cycloolefin resins are no longer out of reach.

Methods

Theoretical Methods

Density functional theory (DFT) calculations were performed to evaluate the thermodynamics of polymerization and de-polymerization using implicit solvent environments of decalin and $CHCl_3$ respectively. All calculations were carried out at the National Energy Research

Scientific Computing facility Cray XC40 computer running an Intel Xeon Processor E5-2698 v3 node with 128 GB of memory. All ground state *ab initio* calculations were performed using Q-Chem version 5.4.1.[65]

To obtain ground state geometries for each molecule in the present study, a conformer search was performed as implemented by the Conformer-Rotamer Ensemble Sampling Tool (CREST)[43] algorithm using a solvent environment of either hexane (polymerization) or $CHCl_3$ (de-polymerization). The lowest energy conformer obtained from CREST was further optimized via DFT using a hybrid generalized gradient approximation (GGA) density functional along with a triple-ζ basis set along with an implicit solvent model modelling either decalin (polymerization) or $CHCl_3$ (depolymerization). This follows an implementation of ωB97X-D hybrid GGA functional[45] using the Ahlrichs' def2-TZVP triple-ζ basis set[46] and the SMD[44] solvent model. Frequency calculations were carried out on the optimized structures using the same B3LYP/def2-TZVP and level of theory to ensure a ground state had been reached as well as to obtain enthalpies.

Energy decomposition analyses (EDA)[51] were carried out between the Ru catalyst and small molecule analogues to investigate poisoning the catalyst by the nitrogen motifs versus the double bond binding to the catalyst. Geometry optimizations and ALMO-EDA[66] calculations of the catalyst-small molecule pair were performed using ωB97X-D range separated hybrid GGA functional[67] with an empirical D3 dispersion correction[68] and using the Ahlrichs' def2-SVPD double-ζ basis set.[46]

bioXL Synthesis

Adipic acid (1.46 g, 10.0 mmol), 1,2,3,4,7,8-hexahydroazocine (2.42 g, 22.0 mmol), TMOS (7.38 mL, 50 mmol) and 2.62 mL toluene was added to a three-neck flask fitted with a reflux condenser

attached to a B14-B19 adapter loosely filled with glass wool and 1 g of activated 4-Å molecular sieves. The mixture was purged under nitrogen for 30 min. The reaction was refluxed overnight and TLC indicated the reaction completion. The mixture was then diluted with 50 mL of THF and the organic phase was washed with 150 mL 0.3 M K_2CO_3 solution. Sodium chloride solid was added to separate the two phases. The aqueous phase was extracted with THF (50 mL×3) and the combined organic phased was dried with anhydrous $MgSO_4$. Evaporate the solvent and the orange crude oil was purified with Biotage automated liquid chromatography using gradient mobile phase from pure ethyl acetate to ethyl acetate/methanol = 3/1 (v/v) (2.15 g, 65%).

Thermal-curing

bioXL (100 mg, 0.15 mmol, 1 eq.), and Grubbs II Catalyst (0.64 mg, 0.5 mol%) was dissolved in 20 μL DCM in the glove box. The solvent was evaporated, and the vial was heated at 60 °C for 12 h. A piece of light brown plastic was obtained. The plastic was swollen in $CHCl_3$ (3 mL) for 3 days ($CHCl_3$ changed every 12 h), and then dried under vacuum under 40 °C heating for 1 day. A gel fraction of 90% was obtained.

Photo-curing

bioXL (100 mg, 0.15 mmol, 1 eq.), HeatMet (0.94 mg, 1 mol%) and ITX (0.57 mg, 1.5 mol%) was dissolved in 20 μL DCM in the glove box. The solvent was evaporated, and the vial was sealed and taken out from the glove box and placed in the middle of the Penn PhD Photoreactor (395 nm, 4 W). The resin cured for 60 min and a piece of deep brown plastic was obtained. The plastic was swollen in $CHCl_3$ (3 mL) for 3 days ($CHCl_3$ changed every 12 h), and then dried under vacuum under 40 °C heating for 1 day. A gel fraction of 93% was obtained.

Depolymerization Studies

Procedure a piece of cured plastic (30 mg) was placed in a 20 mL vial with a stir bar in the glove box and 7.2 mL of $CHCl_3$ containing 1.13 mg (2 mol%) of Grubbs Hoveyda II catalyst was added. The vial was kept at 60 °C for 24 h, after which 100 uL ethyl vinyl ether was added to quench the catalyst and 100 mg Quadrapure TU macroporous particle was added to further remove the catalyst and color. The mixture was filtered, and the solvent was removed to obtain dark brown crude product. The crude product was then purified by silica column chromatography (ethyl acetate: methanol 0%–20%) to recover the original crosslinker in 77% yield. The purity of the recovered crosslinker was then examined by NMR and LC-MS.

Acknowledgements

This material is based upon work supported by the National Science Foundation under Grant 2036849. This Work at the Molecular Foundry—including synthesis and characterization—was supported by the Office of Science, Office of Basic Energy Sciences, of the U.S. Department of Energy under Contract No. DE-AC02-05CH11231. Computation was carried out at the National Energy Research Scientific Computing Center (NERSC), a U.S. Department of Energy Office of Science User Facility operated under the same contract. This work was supported by the Joint BioEnergy Institute (https://www.jbei.org), which is supported by the DOE, Office of Science, Office of Biological and Environmental Research under contract no. DE-AC02-05CH11231. M. H acknowledges support from the U.S. Department of Energy, Office of Science, Office of Basic Energy Sciences, Materials Sciences and Engineering Division for financial support under contract

no. DE-AC02-05- CH11231, Unlocking Chemical Circularity in Recycling by Controlling Polymer Reactivity across Scales program CUP-LBL-Helms to conduct the rheological experiments.

Author Contributions

B.A.H, K.A.P., and J.D.K. contributed to the conceptualization and design of the project. Z. X., Z. W., C.W.C., and P.K. contributed to the crosslinker synthesis. Z.X. and B.A.H. contributed to the methodology of resin preparation, characterization, and chemical recycling. Z.X., M. H and B.A.H. contributed to the rheological characterizations of the resins. J.D.K. supervised and S.K. conducted the biosynthetic analysis. S.K conducted HPLC-MS analysis on the recycled product. K.A.P. supervised and M.X. conducted the computational screening of monomers and EAD analysis. Z.X. and B.A.H. wrote the original draft. All authors contributed to the final draft and editing. B.A.H, J.D.K. and K.A.P. supervised research, provided project administration, and acquired funding.

Conflict of Interest

B.A.H. has a financial interest in Sepion Technologies. J.D.K. has a financial interest in Amyris, Lygos, Demetrix, Napigen, MapleBio, Apertor Labs, Berkeley Yeast, Ansa Biotechnologies and Zero Acre Farms. B.A.H. and J.D.K. have a financial interest in Cyklos Materials. The remaining authors declare no competing interests.

1. Slugovic, C. Industrial applications of olefin metathesis polymerization. in *OlefinMetathesis: Theory and Practice, Grela, K. Ed.* (ed. Grela, K.) 329–333 (Wiley, 2014).

2. Yamazaki, M. Industrialization and application development of cyclo-olefin polymer. *J. Mol. Catal. A Chem.* **213**, 81–87 (2004).

3. Shieh, P. *et al.* Cleavable comonomers enable degradable, recyclable thermoset plastics. *Nature* **583**, 542–547 (2020).

4. Robertson, I. D. *et al.* Rapid energy-efficient manufacturing of polymers and composites via frontal polymerization. *Nature* **557**, 223–227 (2018).

5. Foster, J. C. *et al.* Continuous Additive Manufacturing using Olefin Metathesis. *Adv. Sci.* **9**, 2200770 (2022).

6. Leguizamon, S. C. *et al.* Photoinitiated Olefin Metathesis and Stereolithographic Printing of Polydicyclopentadiene. *Macromolecules* **55**, 8273–8282 (2023).

7. Leguizamon, S. C., Cook, A. W. & Appelhans, L. N. Employing Photosensitizers for Rapid Olefin Metathesis Additive Manufacturing of Poly(dicyclopentadiene). *Chem. Mater.* **33**, 9677–9689 (2021).

8. Davydovich, O. *et al.* Frontal Polymerization of Dihydrofuran Comonomer Facilitates Thermoset Deconstruction. *Chem. Mater.* **34**, 8790–8797 (2022).

9. Piya, S., Shamsuzzoha, A. & Khadem, M. Analysis of supply chain resilience drivers in oil and gas industries during the COVID-19 pandemic using an integrated approach. *Appl. Soft. Comput.* **121**, 108756 (2022).

10. Verbeek, T. & Mah, A. Integration and Isolation in the Global Petrochemical Industry: A Multiscalar Corporate Network Analysis. *Econ. Geogr.* **96**, 363–387 (2020).

11. Sathe, D. *et al.* Olefin metathesis-based chemically recyclable polymers enabled by fused-ring monomers. *Nat. Chem.* **13**, 743–750 (2021).

12. Wu, X. *et al.* Closed-loop recyclability of a biomass-derived epoxy-amine thermoset by methanolysis. *Science (1979)* **384**, (2024).

13. Demarteau, J. *et al.* Biorenewable and circular polydiketoenamine plastics. *Nat. Sustain.* **6**, 1426–1435 (2023).

14. von Vacano, B. *et al.* Sustainable Design of Structural and Functional Polymers for a Circular Economy. *Angew. Chem. Int. Ed* **62**, e202210823 (2023).

15. Nivina, A., Yuet, K. P., Hsu, J. & Khosla, C. Evolution and Diversity of Assembly-Line Polyketide Synthases. *Chem. Rev.* **119**, 12524–12547 (2019).

16. Vougioukalakis, G. C. & Grubbs, R. H. Ruthenium-based heterocyclic carbene-coordinated olefin metathesis catalysts. *Chem. Rev.* **110**, 1746–1787 (2010).

17. Ogba, O. M., Warner, N. C., O'Leary, D. J. & Grubbs, R. H. Recent advances in ruthenium-based olefin metathesis. *Chem. Soc. Rev.* **47**, 4510–4544 (2018).

18. Si, G. & Chen, C. Cyclic–acyclic monomers metathesis polymerization for the synthesis of degradable thermosets, thermoplastics and elastomers. *Nat. Synth.* **1**, 956–966 (2022).

19. Sun, H., Liang, Y., Thompson, M. P. & Gianneschi, N. C. Degradable polymers via olefin metathesis polymerization. *Prog. Polym. Sci.* **120**, 101427 (2021).

20. Feist, J. D. & Xia, Y. Enol Ethers Are Effective Monomers for Ring-Opening MetathesisPolymerization: Synthesis of Degradable and DepolymerizablePoly(2,3-dihydrofuran). *J. Am. Chem. Soc* **142**, 1186–1189 (2020).

21. Leguizamon, S. C. *et al.* Additive Manufacturing of Degradable Materials via Ring-Opening Metathesis Polymerization (ROMP). *ACS Appl. Mater. Interfaces* **14**, 51301–51306 (2022).

22. Huang, B. *et al.* Backbone-Photodegradable Polymers by Incorporating Acylsilane Monomers via Ring-Opening Metathesis Polymerization. *J. Am. Chem. Soc.* **143**, 17920–17925 (2021).

23. Sathe, D., Yoon, S., Wang, Z., Chen, H. & Wang, J. Deconstruction of Polymers through Olefin Metathesis. *Chem. Rev.* (2023) doi:10.1021/ACS.CHEMREV.3C00748.

24. Ibrahim, T. *et al.* Chemical recycling of polyolefins via ring-closing metathesis depolymerization. *Chem. Commun.* **60**, 1361–1371 (2024).

25. Ibrahim, T., Martindale, J., Ritacco, A., Rodriguez, M. & Sun, H. Polyheptenamer: A chemically recyclable polyolefin enabled by the low strain of seven-membered cycloheptene. *J. Polym. Sci.* (2024) doi:10.1002/POL.20240196.

26. Zhou, J., Sathe, D. & Wang, J. Understanding the Structure–Polymerization Thermodynamics Relationships of Fused-Ring Cyclooctenes for Developing Chemically Recyclable Polymers. *J. Am. Chem. Soc.* **144**, 928–934 (2022).

27. Choi, K. & Hyeok Hong, S. Chemically recyclable oxygen-protective polymers developed by ring-opening metathesis homopolymerization of cyclohexene derivatives. *Chem* **9**, 2637–2654 (2023).

28. Chen, H., Shi, Z., Hsu, T. G. & Wang, J. Overcoming the Low Driving Force in Forming Depolymerizable Polymers through Monomer Isomerization. *Angew. Chem. Int. Ed.* **60**, 25493–25498 (2021).

29. Zhou, J., Sathe, D. & Wang, J. Understanding the Structure–Polymerization Thermodynamics Relationships of Fused-Ring Cyclooctenes for Developing Chemically Recyclable Polymers. *J. Am. Chem. Soc.* **144**, 928–934 (2022).

30. Neary, W. J., Isais, T. A. & Kennemur, J. G. Depolymerization of Bottlebrush Polypentenamers and Their Macromolecular Metamorphosis. *J. Am. Chem. Soc.* **141**, 14220–14229 (2019).

31. Shi, C., Clarke, R. W., McGraw, M. L. & Y-X Chen, E. Closing the“One Monomer−Two Polymers−One Monomer”Loopvia Orthogonal (De)polymerization of a Lactone/Olefin Hybrid. *J. Am. Chem. Soc* **144**, 2264–2275 (2022).

32. Naguib, M. & Yassin, M. A. Polymeric Antioxidant via ROMP of Bioderived Tricyclic Oxanorbornene Based on Vanillin and Furfurylamine. *ACS Appl. Polym. Mater.* **4**, 2181–2188 (2022).

33. Meronuck, R. A., Steele, J. A., Mirocha, C. J. & Christensen, C. M. Tenuazonic Acid, a Toxin Produced by Alternaria alternata . *Appl. Microbiol* **23**, 613–617 (1972).

34. Boudreau, P. D. *et al.* Expanding the Described Metabolome of the Marine Cyanobacterium Moorea producens JHB through Orthogonal Natural Products Workflows. *PLoS One* **10**, e0133297 (2015).

35. Mohanraj, S., Subramanian, P. S. & Herz, W. Minor alkaloids of Heliotropium curassavicum. *Phytochemistry* **21**, 1775–1779 (1982).

36. Tsutsumi, H. *et al.* Unprecedented Cyclization Catalyzed by a Cytochrome P450 in Benzastatin Biosynthesis. *J. Am. Chem. Soc.* **140**, 6631–6639 (2018).

37. Wang, D. S. ; F. L. H. ; F. D. G. H. *Natural Small Molecule Drugs from Plants*. vol. 5 (2018).

38. Kaltenegger, E. *et al.* Insecticidal pyrido[1,2-a]azepine alkaloids and related derivatives from Stemona species. *Phytochemistry* **63**, 803–816 (2003).

39. Hu, Z. X. *et al.* Aloperine-Type Alkaloids with Antiviral and Antifungal Activities from the Seeds of Sophora alopecuroides L. *J. Agric. Food. Chem.* **72**, 8225–8236 (2024).

40. Gomez-Escribano, J. P. *et al.* Structure and biosynthesis of the unusual polyketide alkaloid coelimycin P1, a metabolic product of the cpk gene cluster of Streptomyces coelicolor M145. *Chem. Sci.* **3**, 2716–2720 (2012).

41. Zúñiga, G. E., Tapia, A., Arenas, A., Contreras, R. A. & Zúñiga-Libano, G. Phytochemistry and biological properties of Aristotelia chilensis a Chilean blackberry: a review. *Phytochem. Rev.* **16**, 1081–1094 (2017).

42. Seibel, E. *et al.* Genome mining for macrolactam-encoding gene clusters allowed for the network-guided isolation of β-amino acid-containing cyclic derivatives and heterologous production of ciromicin A. *Commun. Chem.* **6**, 257 (2023).

43. Pracht, P., Bohle, F. & Grimme, S. Automated exploration of the low-energy chemical space with fast quantum chemical methods. *Phys. Chem. Phys. Chem.* **22**, 7169–7192 (2020).

44. Marenich, A. V., Cramer, C. J. & Truhlar, D. G. Universal solvation model based on solute electron density and on a continuum model of the solvent defined by the bulk dielectric constant and atomic surface tensions. *J. Phys. Chem. B.* **113**, 6378–6396 (2009).

45. Chai, J. Da & Head-Gordon, M. Long-range corrected hybrid density functionals with damped atom–atom dispersion corrections. *Phys. Chem. Chem. Phys* **10**, 6615–6620 (2008).

46. Weigend, F. & Ahlrichs, R. Balanced basis sets of split valence, triple zeta valence and quadruple zeta valence quality for H to Rn: Design and assessment of accuracy. *Phys. Chem. Phys. Chem.* **7**, 3297–3305 (2005).

47. Schleyer, P. V. R., Wiliiams, J. E. & Blanchard, K. R. The Evaluation of Strain in Hydrocarbons. The Strain in Adamantane and its Origin. *J. Am. Chem. Soc.* **92**, 2377–2386 (1970).

48. Kuanr, N., Gilmour, D. J., Gildenast, H., Perry, M. R. & Schafer, L. L. Amine-Containing Monomers for Ring-Opening Metathesis Polymerization: Understanding Chelate Effects in Aryl- and Alkylamine-Functionalized Polyolefins. *Macromolecules* (2021) doi:10.1021/ACS.MACROMOL.1C02664.

49. Perry, M. R. *et al.* Catalytic synthesis of secondary amine-containing polymers: Variable hydrogen bonding for tunable rheological properties. *Macromolecules* **49**, 4423–4430 (2016).

50. Cormier, S. K. & Fogg, D. E. Probing Catalyst Degradation in Metathesis of Internal Olefins: Expanding Access to Amine-Tagged ROMP Polymers. *ACS Catal.* **13**, 11834–11840 (2023).

51. Phipps, M. J. S., Fox, T., Tautermann, C. S. & Skylaris, C.-K. Energy decomposition analysis approaches and their evaluation on prototypical protein-drug interaction patterns †. *Chem. Soc. Rev.* **44**, 3177 (2015).

52. Liu, X. *et al.* Biosynthetic Pathway and Metabolic Engineering of Succinic Acid. *Front. bioeng. biotechnol.* **10**, 843887 (2022).

53. Han, T., Kim, G. B. & Lee, S. Y. Glutaric acid production by systems metabolic engineering of an L-lysine–overproducing Corynebacterium glutamicum. *PNAS* **117**, 30328–30334 (2020).

54. Hagen, A. *et al.* Engineering a Polyketide Synthase for in Vitro Production of Adipic Acid. *ACS Synth. Biol.* **5**, 21–27 (2016).

55. Yu, J. Le, Xia, X. X., Zhong, J. J. & Qian, Z. G. A novel synthetic pathway for glutarate production in recombinant Escherichia coli. *Process Biochem.* **59**, 167–171 (2017).

56. Kruyer, N. S., Wauldron, N., Bommarius, A. S. & Peralta-Yahya, P. Fully biological production of adipic acid analogs from branched catechols. *Sci. Rep* **10**, 13367 (2020).

57. Haushalter, R. W. *et al.* Production of Odd-Carbon Dicarboxylic Acids in Escherichia coli Using an Engineered Biotin-Fatty Acid Biosynthetic Pathway. *J. Am. Chem. Soc.* **139**, 4615–4618 (2017).

58. Dellomonaco, C., Clomburg, J. M., Miller, E. N. & Gonzalez, R. Engineered reversal of the β-oxidation cycle for the synthesis of fuels and chemicals. *Nature* **476**, 355–359 (2011).

59. Bowen, C. H., Bonin, J., Kogler, A., Barba-Ostria, C. & Zhang, F. Engineering Escherichia coli for Conversion of Glucose to Medium-Chain ω-Hydroxy Fatty Acids and α,ω-Dicarboxylic Acids. *ACS Synth. Biol.* **5**, 200–206 (2016).

60. Braddock, D. C. *et al.* Tetramethyl Orthosilicate (TMOS) as a Reagent for Direct Amidation of Carboxylic Acids. *Org. Lett.* **20**, 950–953 (2018).

61. Jacobson, H., Stockmayer, W. H., Jacobson, H., Stockmayer, W. H. & Acobson, H. J. Intramolecular Reaction in Polycondensations. I. The Theory of Linear Systems. *J. Chem. Phys.* **18**, 1600–1606 (1950).

62. Kuhn, K. M. *et al.* Low catalyst loadings in olefin metathesis: Synthesis of nitrogen heterocycles by ring-closing metathesis. *Org. Lett.* **12**, 984–987 (2010).

63. Bates, J. M., Lummiss, J. A. M., Bailey, G. A. & Fogg, D. E. Operation of the boomerang mechanism in olefin metathesis reactions promoted by the second-generation Hoveyda catalyst. *ACS Catal.* **4**, 2387–2394 (2014).

64. Suslick, B. A., Alzate-Sanchez, D. M. & Moore, J. S. Scalable Frontal Oligomerization: Insights from Advanced Mass Analysis. *Macromolecules* **55**, 8234–8241 (2022).

65. Epifanovsky, E. *et al.* Software for the frontiers of quantum chemistry: An overview of developments in the Q-Chem 5 package. *J. Chem. Phys.* **155**, 84801 (2021).

66. Khaliullin, R. Z., Cobar, E. A., Lochan, R. C., Bell, A. T. & Head-Gordon, M. Unravelling the origin of intermolecular interactions using absolutely localized molecular orbitals. *J. Phys. Chem. A* **111**, 8753–8765 (2007).

67. Mardirossian, N. & Head-Gordon, M. ωB97X-V: A 10-parameter, range-separated hybrid, generalized gradient approximation density functional with nonlocal correlation, designed by a survival-of-the-fittest strategy. *Phys. Chem. Chem. Phys.* **16**, 9904–9924 (2014).

68. Grimme, S., Antony, J., Ehrlich, S. & Krieg, H. A consistent and accurate ab initio parametrization of density functional dispersion correction (DFT-D) for the 94 elements H-Pu. *J. Chem. Phys.* **132**, 154104 (2010).